
Article:
Khan, M.A. orcid.org/0000-0002-4219-2149, Sun, J., Li, B. et al. (2 more authors) (2021) Magnetic sensors-a review and recent technologies. Engineering Research Express, 3 (2). 022005. ISSN 2631-8695

https://doi.org/10.1088/2631-8695/ac0838

Magnetic sensors-A review and recent technologies

To cite this article: Mohammed Asadullah Khan *et al* 2021 *Eng. Res. Express* **3** 022005

Engineering Research Express

OPEN ACCESS

RECEIVED
26 March 2021

REVISED
17 May 2021

ACCEPTED FOR PUBLICATION
4 June 2021

PUBLISHED
15 June 2021

TOPICAL REVIEW

Magnetic sensors-A review and recent technologies

Mohammed Asadullah Khan[1,2], **Jian Sun**[3], **Bodong Li**[4], **Alexander Przybysz**[1] and **Jürgen Kosel**[1,5,*]

[1] Computer, Electrical and Mathematical Science and Engineering division (CEMSE), King Abdullah University of Science and Technology, Thuwal, Saudi Arabia
[2] Department of Automatic Control and Systems Engineering (ACSE), The University of Sheffield, Sheffield, United Kingdom
[3] School of Physics and Electronics, Central South University, Changsha, Hunan, People's Republic of China
[4] EXPEC Advanced Research Centre, Saudi Aramco, Dhahran, Saudi Arabia
[5] Sensor Systems Division, Silicon Austria Labs, Villach, Austria
[*] Author to whom any correspondence should be addressed.

E-mail: jurgen.kosel@kaust.edu.sa

Keywords: magnetic sensors, solid state sensors, flexible, stretchable, internet of things, sensor networks, ubiquitous sensing

Abstract

Magnetic field sensors are an integral part of many industrial and biomedical applications, and their utilization continues to grow at a high rate. The development is driven both by new use cases and demand like internet of things as well as by new technologies and capabilities like flexible and stretchable devices. Magnetic field sensors exploit different physical principles for their operation, resulting in different specifications with respect to sensitivity, linearity, field range, power consumption, costs etc. In this review, we will focus on solid state magnetic field sensors that enable miniaturization and are suitable for integrated approaches to satisfy the needs of growing application areas like biosensors, ubiquitous sensor networks, wearables, smart things etc. Such applications require a high sensitivity, low power consumption, flexible substrates and miniaturization. Hence, the sensor types covered in this review are Hall Effect, Giant Magnetoresistance, Tunnel Magnetoresistance, Anisotropic Magnetoresistance and Giant Magnetoimpedance.

1. Introduction

The development of magnetic sensors has been a pursuit of human endeavor since centuries past. The driving force behind this, for a long time, was sensing the geomagnetic field for the purpose of navigation. This led to the invention of the magnetic compass, following which, mankind was no longer beholden to the stars to guide them across the treacherous oceans. This single invention resulted in a monumental period of growth, prosperity and progress. It is a testament to the versatility and sheer timelessness of this sensor that it still persists to this day in the form of miniaturized solid-state magnetic sensors that alongside other sensors enable vehicle (ships, aeroplanes, automobiles) as well as personal navigation using smartphones and wearable smart devices such as smartwatches [1, 2].

The exploration of the intrinsic link between electricity and magnetism in the 19th century [3–6] led to the discovery of other physical phenomena that could be used to sense magnetism. This culminated in a plethora of magnetic sensors, which are used for measuring other properties such as pressure, proximity, position, fluid flow, etc Today, these sensors are an indispensable component of the internet of things, which has numerous applications in fields as diverse as wearable technology, consumer electronics, healthcare, navigation, agriculture, animal husbandry, etc The global magnetic sensor industry revenue is expected to exceed 2.5 billion dollars in 2022 [7], driven by growth in automotive, industrial and biomedical sectors.

Magnetic sensors have been developed utilizing various physical phenomena such as Electromagnetic Induction, Hall Effect, Tunnel Magnetoresistance(TMR), Giant Magnetoresistance (GMR), Anisotropic Magnetoresistance (AMR) and Giant Magnetoimpedance (GMI) [8]. For applications, where highest sensitives are required, superconducting quantum interference devices (SQUID) are the first choice [9]. Induction based coil type sensors are usually bulky and robust and find application in industrial sensing systems. However, these

sensors are not easily miniaturizable due to the difficulty in fabricating 3D coils and the poor performance of planar coils compared to their wire wound counterparts. SQUID sensors require cooling down to low temperatures, and even with the advent of high-temperature superconductors, they involve high costs and complexity and only allow some of their components to be miniaturized [10]. On the other hand, solid-state Hall effect, GMR, TMR, AMR and GMI sensors are manufactured using planar microfabrication processes and are capable of offering high sensitivity in a relatively compact footprint. The compatibility of solid-state magnetic sensors with complementary metal-oxide-semiconductor (CMOS) fabrication processes makes it feasible to achieve integration of sensor with sensing and computing circuitry at the same time, resulting in systems on chip, which are highly attractive for internet of things applications. Further, Hall and magnetoresistance sensors comprise 98% of the magnetic sensor market [7]. Especially, MR sensors are predicted to proliferate in the areas of biomedical applications, flexible electronics, position sensing/human-computer interaction, non-destructive evaluation and monitoring, and navigation and transportation, due to improvements in sensing and operational performance [11]. Hence, out of the many different kinds of magnetic field sensors, this review will focus on the latest advances and applications of Hall effect, GMR, TMR, AMR, GMI sensors.

Attention will be paid in particular to the development of flexible and conformal magnetic sensors. Over the past few years flexible electronics has resulted in novel applications in the fields of healthcare, entertainment and consumer electronics. This led to the emergence of a robust and rapidly growing market, estimated to be worth $7.6 Billion by 2027 [12]. In this environment, the development of flexible magnetic sensors is attractive for commercial purposes as well as for enabling new application areas. Different methods such as substrate thinning, polymeric substrates and inkjet printing are used for fabrication of flexible sensors. Existing flexible magnetic sensors, their fabrication methods and performance will be studied in this review. This review also emphasizes magnetic sensors that are being deployed in the healthcare sector for both therapeutic as well as diagnostic purposes. Novel approaches to investigating medically relevant phenomena, organisms, cells and chemicals using magnetic sensors will also be included.

2. Hall effect sensors

2.1. Background

Hall effect sensors are transducers measuring magnetic fields based on the principle of the Hall effect that effect was discovered in 1879 by the American physicist Edwin Herbert Hall in gold leaves [13]. It is a result of the magnetic Lorentz force, which deflects moving charge carriers that constitute the electric current in a magnetic field.

In a solid conductor placed in a magnetic field $\boldsymbol{B}$, the magnetic Lorentz force acting on a single charge carrier can be expressed as

$$F = qv\ x\ B \tag{1}$$

where q is the charge of the carrier. And v is the instantaneous drift velocity vector of the moving carrier which is calculated as

$$v = I/(nqwd) \tag{2}$$

with $\boldsymbol{I}$ being the applied current and w and d being the width and thickness of the conductor, respectively.

When a magnetic field is applied in the direction perpendicular to the current flow, the magnetic Lorentz force causes a deflection of the current. As a consequence, charges of opposite sign accumulate at two surfaces or edges of the conductor orthogonal to the current flow (figure 1), leading to a differential voltage, i.e. the Hall voltage $\boldsymbol{V}_H$. When an equilibrium state is reached,

$$qv\ x\ B = V_H q/w \tag{3}$$

The value of V_H can be expressed in terms of I and B as

$$V_H = (IB)/(nqd) \tag{4}$$

In case of a n-type/p-type conductor, V_{H} is then negative/positive with the positive values of I and B.

The key parameter determining the sensitivity of a Hall effect sensor is the carrier mobility μ of its building material [14]. For a long time after the Hall effect was discovered, it was only utilized in material classification. Until 1950's, with the development of semiconductor materials, i.e. the III-V compounds (e.g. InAs with $\mu \sim 20{,}000\ \mathrm{cm^2\,Vs^{-1}}$, GaAs with $\mu \sim 8{,}000\ \mathrm{cm^2\,Vs^{-1}}$, InSb with $\mu \sim 60{,}000\ \mathrm{cm^2\,Vs^{-1}}$), Hall effect sensors were firstly introduced in laboratories as magnetic measurement instruments. Nowadays, silicon-based Hall sensors are dominating the market albeit with a low mobility of $\sim 1{,}000\ \mathrm{cm^2\,Vs^{-1}}$. These sensors benefit from a mature silicon CMOS technology, which enables efficient monolithic fabrication of the sensing element and other

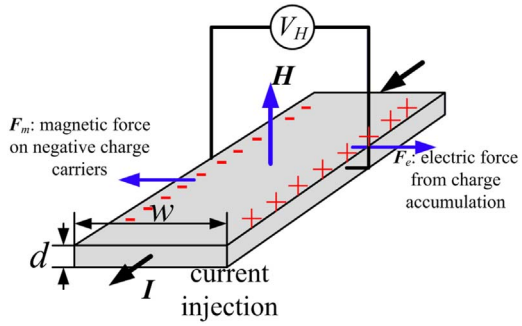

Figure 1. Schematic view of a bar (n-type) Hall device. A current, *I*, is applied along the bar as well as a magnetic field, *B*, perpendicular to the surface, which gives rise to a Hall voltage, V_H. Note that the direction of the current *I* in the diagram is that of conventional current, so that the motion of electrons is in the opposite direction.

processing electronics. The silicon-based Hall sensors have a typical sensitivity of $100 \sim 1000$ V $A^{-1}T^{-1}$, a resolution of ~1000 nT/$\sqrt{\text{Hz}}$, and an offset of ~10 mT [15, 16]. For applications that require a higher sensitivity of >1000 V $A^{-1}T^{-1}$, better resolution of ~100 nT/$\sqrt{\text{Hz}}$ and a lower offset of ~1 mT, Hall sensors based on high mobility III/V semiconductors GaAs, InAs, and their 2-dimensional electron gases are necessary though at much higher expense [17, 18]. More recently, the rise of graphene has brought new opportunities to Hall effect sensors [19–22]. A record-high sensitivity of 5700 V $A^{-1}T^{-1}$ and resolution 50 nT/$\sqrt{\text{Hz}}$ have been demonstrated in the laboratory with a prototype graphene Hall sensor [23].

Hall effect sensors possess a number of advantages: simple device architecture, easy manufacture, low cost; possibility of scaling down and integration with CMOS circuits; linear response; highly repeatable operation, and excellent robustness.

However, Hall effect sensors suffer from several shortcomings. The output signal is weak compared to, e.g. MR sensors; they drift with temperature, and have a finite offset signal. To overcome these problems, most commercially available Hall effect sensors are manufactured with sophisticated electronic circuits to provide constant current, amplify the output voltage, compensate drift, correct offset, digitize signal, and perform signal processing.

2.2. Applications

In general, the applications of Hall effect sensors are classified into two main categories, i.e. the linear output Hall sensors and digital output Hall effect sensors or the Hall effect switches [14].

Linear output Hall sensors measure the magnitude of the magnetic field and output a linear signal, and they are commonly used in current and position sensing. They can be found in a wide range of applications, such as disk drives, motor control indicators, power supply protection, pressure diaphragms, flow meters, damper controls, brushless DC motors, rotary encoders, ferrous metal detectors, vibration sensors, tachometers, etc [14].

Digital Hall sensors operate as electronic switches. Typically, they are designed to be 'OFF' at no magnetic field. When an applied magnetic field exceeds a pre-set value, the output of the digital Hall sensor switches to the 'ON' state without any contact bounce. Such a switch costs less than a mechanical switch and is more reliable under severe conditions. Common applications include: rotation speed detectors, pulse counters in printers and motor drives, valve position sensors, joy stick sensors, door interlocks, proximity detectors, lens position sensors, paper sensors, shaft position sensors, etc [14].

In additional to these aforementioned applications in commercial electronics and industries, Hall sensors have also been widely studied and employed in the emerging areas of biomedical sensing and wearable electronics.

Reproduced with permission from [24].

Recent advances in microfluidics and lab-on-chip technology boost the development of the compact medical diagnostic and bioscreening systems. Miniaturized Hall sensors have the advantages of low cost, simple integration, and no interference by complex biomedical samples are commonly employed as a biosensor using magnetic labels. Thereby, the Hall sensor detects the magnetic nanoparticles, which label biological specimens, by measuring their stray fields of $\mu T \sim$ mT in an external magnetic field [25–30].

Conventional Hall sensors are thick and rigid, limiting their applicability in the field of flexible and wearable electronics. Recently, flexible Hall sensors have been demonstrated on bendable and stretchable polymeric substrates [31–34]. For instance, Bismuth thin film-based Hall sensors were made on polyimide (PI) substrates. They exhibited a relatively low sensitivity of 2.3 V $A^{-1}T^{-1}$ which they maintained for at least 50 bending cycles to a radius of 8 mm [32]. A magnetic Permalloy-based planar Hall sensor was made on polyethylenterephthalat (PET) capable to detect sub-200 nT fields with a high sensitivity of 172 V $A^{-1}T^{-1}$ (with 5 mA bias current) and

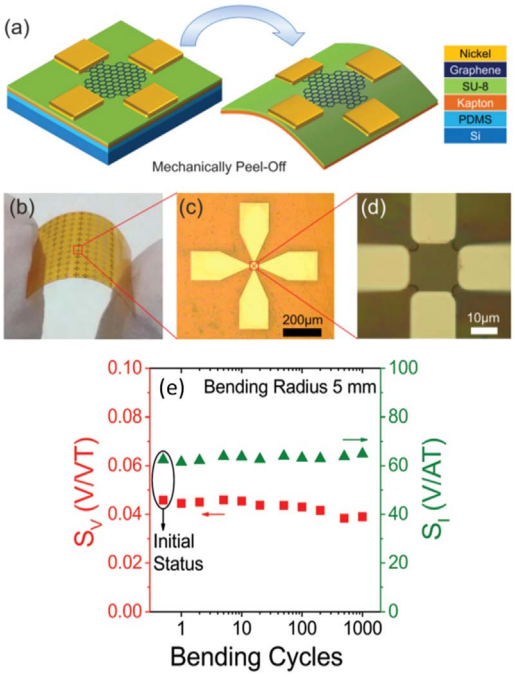

Figure 2. A representative graphene-based flexible Hall sensor. (a), (c), (d) Device structure, (b) Device bendability, and (e) the sensitivity evolution of the graphene flexible Hall sensor subjected to 1000 cycles of bending. Reproduced from [35] with permission of The Royal Society of Chemistry.

an extremely high resolution of 1.5 nT/ $Hz^{0.5}$, which is on par with the state-of-the-art commercially available rigid devices [31]. An excellent bending stability has been highlighted by the negligible 0.3% output fluctuation after more than 150 bending cycles to the radius lower than 1 mm. In addition, the emergence of two-dimensional graphene has also greatly promoted the applications of flexible Hall sensors with its outstanding mechanical flexibility [32, 35, 24] (figure 2). For example, an excellent flexibility with only 0.6% performance degradation after 1000 bending cycles to a radius of 5 mm has been shown for graphene Hall sensors on Kapton foil with a high sensitivity of 79 $V A^{-1}T^{-1}$.

These encouraging results are promising for upcoming applications in fields such as soft robotics, wearable electronics and electronic skin. Together with their robustness, easy fabrication, straigth forward integration with CMOS, and low cost, Hall sensors will continue to play a dominant role in the global magnetic sensor market with a high share for a long time in the future.

3. Anisotropic magnetoresistance

3.1. Background

The resistance of certain materials is dependent on the angle between the direction of the applied current and the magnetization of the material itself. This phenomenon is called anisotropic magnetoresistance (AMR). It was first discovered by Lord Kelvin in 1856, who reported that ferromagnetic metals (Fe and Ni) exhibit higher resistance, when magnetized parallel to the current, and minimum resistance, when the magnetization is perpendicular to the current [36]. It was observed that the magnetoresistance was thrice as strong in Nickel than in Iron. The effect arises due to magnetization direction dependent scattering of conducting electrons with uncompensated spins. While any simple bar of ferromagnetic material will exhibit AMR, the effect is non-linear with respect to field strength. Considering the case of a ferromagnetic structure with maximum resistance of R_{max}, when the magnetization and the current are parallel, and minimum resistance of R_{min}, when the magnetization and current are orthogonal. Thus, the change in resistance is given by $\Delta R = R_{max}.-.R_{min}$. If this structure has a total magnetic anisotropy field, H_{an}, and applied external field, H_{app}, then the resistance is given as [37, 38]

$$R = R_{max} - \Delta R\left(\frac{H_{app}}{H_{an}}\right)^2 \tag{5}$$

Thus, the resistance of a simple ferromagnetic structure varies non-linearly with the applied field. Further, when the applied field is small ($H_{app} << H_{an}$), the sensitivity of the sensor becomes extremely small. Using an external bias field or a conducting structure, which rotates the direction of the current by 45° with respect to the

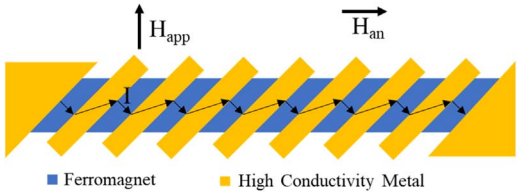

Figure 3. Barber-pole structure twists the current direction at an angle to the anisotropy field, linearizing the dependence of magnetoresistance on the applied field.

easy axis of the material are potential solutions to linearize this effect. One method is to use a V-shaped strip of ferromagnetic material and another method is to use a barber pole structure (figure 3), made by depositing strips of a good conductor on top of the ferromagnetic material and at an angle of 45° to it. In the latter method, the current prefers travelling in the good conductor than in the ferromagnet, the direction of current in the ferromagnetic material is rotated at 45° to the plane of the applied field. The field dependent resistance equation for such structure is given by

$$R = R_0 + \Delta R \frac{H_{app}}{H_{an}} \sqrt{1 - \left(\frac{H_{app}}{H_{an}}\right)^2} \tag{6}$$

For low values of applied magnetic field i.e. $H_{app} < H_{an}/2$, the barber pole structure resistance expression exhibits less than 5% non-linearity.

The most popularly used material for AMR sensors is Permalloy, an alloy of iron and nickel. In particular, the $Ni_{0.81}Fe_{0.19}$ composition is relevant, as it offers low coercivity and negligible magnetostriction [39]. AMR sensors have lower sensitivity than GMR and TMR sensors, however they also are far easier to fabricate, offer flexibility in device shape and resistance and have better signal-to-noise ratio at low frequencies [40–42].

3.2. Applications

Owing to its simple fabrication process, AMR sensors continue to be utilized for new sensor developments. Its miniaturization is straight forward, and the robust structure allows its fabrication on a variety of substrates, including flexible and stretchable ones.

The usage of AMR sensor with a micropatterned gas channel and a biasing magnet to detect oxygen is presented in [43]. Oxygen is paramagnetic and has greater susceptibility than any other gas in the environment, which makes this sensor highly selective. The AMR sensor can be used to detect oxygen content between 0% and 100%. AMR sensors also find applications in linear positioning systems, due to their robustness [44, 45]. Using a 3 axis AMR sensor in conjunction with an elastic dome mechanically coupled with a permanent magnet, a tactile sensor is presented in [46]. This sensor delivered a sensitivity of 58 mV N^{-1} to normal force and 78 mV N^{-1} to shear force. In [47], out of plane sensitivity is imparted to a conventional Permalloy AMR sensor by patterning a grid of Ni micropillars on top of it, which serve as flux concentrators converting the out of plane magnetic field into an in-plane field. The sensor delivers a sensitivity of 84 μV/Oe and a resolution of 47 mOe/$(Hz)^{1/2}$ to the out of plane component, which makes it suited for magnetic compass applications. Using a quadruple Permalloy layer AMR sensor, an angular position sensor is designed in [48]. The easy axes of the four Permalloy layers are aligned at different angles (0°, 90°, 45°, 135°), resulting in an AMR stack, which is effectively isotropic in terms of magnetic anisotropy, making this sensor more accurate than conventional single layer AMR sensors, especially at low sensing bias fields (< 100 Oe). An AMR based nuclear magnetic resonance (NMR) system is reported in [49], which has sensitivity and detection limits comparable with microcoils in superconducting magnet based systems. In the field of non-destructive testing, an AMR sensor system is used in [50], implementing multi-frequency eddy current testing to identify defects in an Cu-Cr-Zr alloy used to make rocket nozzles.

Flexible AMR sensors have been demonstrated on a variety of substrates. For example, on 7 μm thick polymer foil [51]. The polymer was spin coated on a Si wafer and a meander shaped Permalloy ($Ni_{0.81}Fe_{0.19}$) sputtered film served as the AMR sensor. The Si wafer was subsequently selectively etched using deep reactive ion etching (DRIE), forming the AMR sensor on flexible polymer foil suspended on a Si frame (figure 4). While, this sensor itself is flexible the packaging process (Si frame) renders it rigid.

In [38], a flexible Permalloy ($Ni_{0.81}Fe_{0.19}$) AMR sensor on a polyethylene terephthalate (PET, 100 μm thickness) substrate, employing the aforementioned barber pole topology is reported. One major challenge with designing flexible magnetic sensors on polymer substrates is the higher surface roughness (when compared to conventional oxidized Si rigid substrate), which causes domain wall pinning, increasing hysteresis and reducing the magnetoresistive effect [52]. This issue is overcome by coating the PET layer with a smooth layer of cured

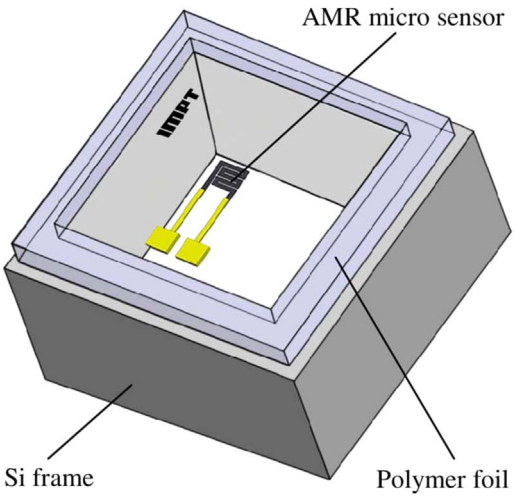

Figure 4. AMR sensor fabricated on polymer foil. The Si frame hinders the flexibility of this design. © [2012] IEEE. Reprinted, with permission, from [51].

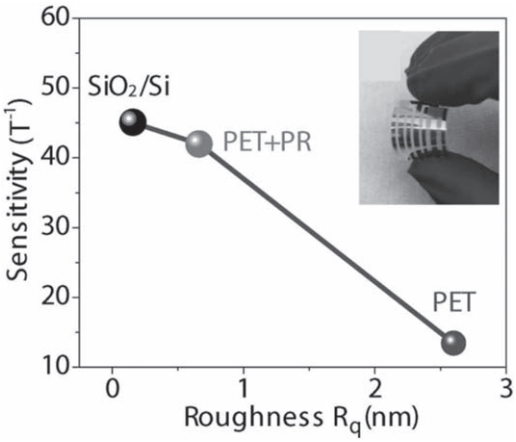

Figure 5. Effect of substrate roughness on sensitivity of flexible AMR sensor. The inset depicts the bending of the sensor. John Wiley & Sons. [© 2016 WILEY-VCH Verlag GmbH & Co. KGaA, Weinheim] [38].

photoresist. Selectively patterned gold is used to form the contacts and the barber pole structure. The sensor has a resolution of 150 nT and a sensitivity of 4200 ppm/Oe (which is quite close to that obtained using a similar AMR sensor on a rigid oxidized Si substrate) (figure 5). It is capable of working when bent at a radius as small as 10 mm and can recover functionality after being bent to a radius of 5 mm.

Permalloy sputtered on paper is another interesting method to create flexible magnetic sensors [53] (figure 6). Combining this sensor with origami to exploit paper's ease of foldability makes this an interesting alternative approach to flexibility, compared to the usual polymer substrate-based sensors. The high surface roughness of paper [2 μm) results in 60% lesser sensitivity than a similar sensor fabricated on rigid oxidized silicon.

AMR sensors are integrated with a microfluidic channel in [54] to allow real time detection of 9 μm magnetic beads. This system could potentially be used for cytometry. One of the principle problems in magnetic microfluidic systems based on superparamagnetic nanobeads is transporting the beads to the sensor. In [55], an L-shaped permalloy AMR strip with two terminating disks is presented. In this structure, it is possible to magnetically inject a transverse head to head domain wall (TDW), at the corner, which in turn becomes a magnetic trap for the nanobeads (figure 7). The trapped beads are then sensed through change in resistivity. A single nanobead (300 nm diameter) was detected by this method. A disposable card based system incorporating an AMR sensor to detect the 16 SRNA gene in the DNA of the bacterium Streptococcus suis is demonstrated in [56].

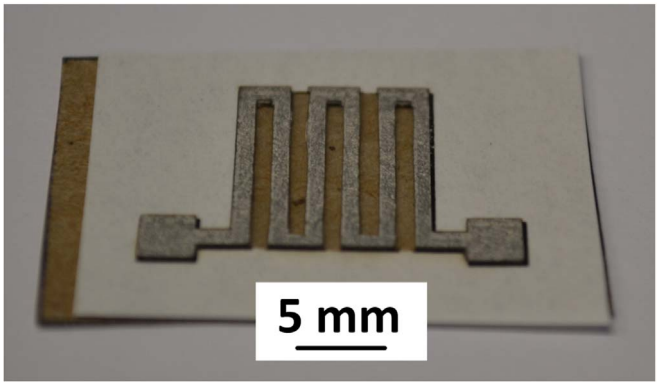

Figure 6. Paper based AMR sensor. Reproduced with permission from [53]. © 2018 Meriem Akin *et al*.

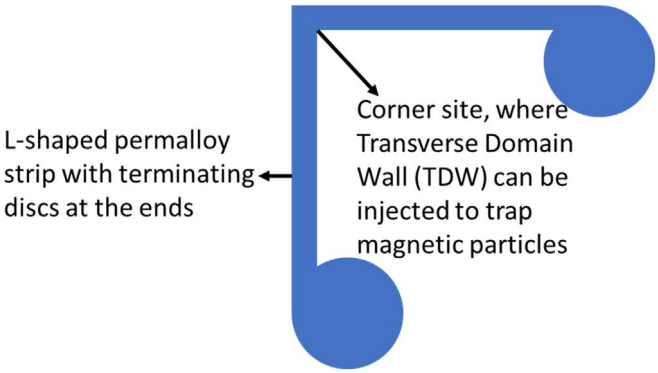

Figure 7. Schematic of L-shaped AMR sensor, where the corner serves as a magnetic particle trap. Reproduced from [55] © IOP Publishing Ltd. All rights reserved.

4. Giant Magnetoresistance

4.1. Background

In a thin film structure composed of a non-magnetic metal layer sandwiched between two magnetic layers, the resistance of the stack changes, depending on the relative orientation of magnetization of the two magnetic layers (figure 8). This effect is a product of spin dependent scattering of electrons. When the magnetization of the two layers is in the same direction, only electrons with one spin polarization are strongly scattered, minimizing the resistance of this heterostructure. Conversely, when the magnetization of the layers is in opposite directions, electrons with both up and down spin polarizations are strongly scattered resulting in large resistance. Albert Fert and Peter Grunberg both independently discovered this phenomenon [57, 58] and for this discovery, they were jointly awarded the 2007 Nobel Prize in Physics. The GMR effect is seen in both possible directions of conduction i.e. from top to bottom (or vice-versa) and across the three layers from left to right (and vice-versa).

In a typical GMR spin valve sensor, one of the two magnetic layers is fabricated to have a fixed direction of magnetization and this layer is called a pinned (or reference) layer. The other layer is called a free layer (figure 9). It is made of a soft magnetic material and the direction of magnetization of this layer rotates under the influence of the applied magnetic field. In case of a GMR device with minimum resistance R_{min} and maximum resistance R_{max}, the MR ratio of the device is given by

$$MR\ ratio = \frac{R_{max} - R_{min}}{R_{min}} \tag{7}$$

When a magnetic field is applied it changes the orientation of the free layer. Assuming that the pinned layer is oriented at an angle of θ_p and the free layer is oriented at θ_f, the resistance of the GMR device [59] can be empirically expressed as

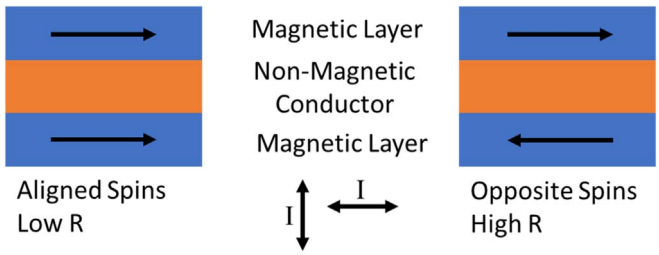

Figure 8. Giant Magnetoresistance Sensor schematic, depicting the allowed directions of conduction.

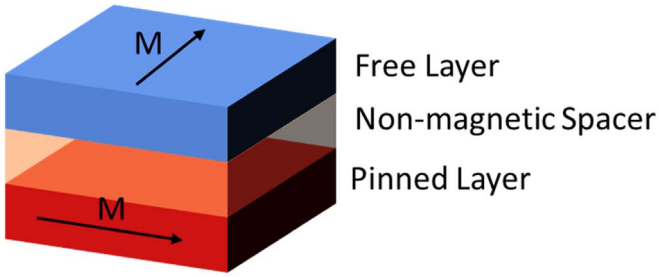

Figure 9. GMR sensor configuration for linear response.

$$R = R_{min} + \frac{R_{min}\, MR\, [1 - \cos(\theta_f - \theta_p)]}{2} \tag{8}$$

If the free layer is aligned orthogonally to the pinned layer as depicted in figure 8, the above equation reduces to

$$R = R_{min} + \frac{R_{min}\, MR\, [1 - \sin(\theta_f)]}{2} \tag{9}$$

Thus, the resistance of the GMR device is proportional to the sine of the angle by which the free layer rotates under the influence of the applied field. For lower applied fields, $\sin(\theta_f)$ varies linearly with the magnetic field strength, thus the output of the sensor is linearized which is desirable for most sensor applications [60].

The free layer is usually fabricated using a soft magnetic material such as CoFeB or NiFe. The magnetization of a ferromagnetic metal in contact with an anti-ferromagnetic metal gets pinned and this phenomenon is exploited to form the pinned/reference layer. However, exchange bias coupling with the free layer leads to an asymmetrical reversal of magnetoresistance with respect to the applied field, which is an undesirable trait [61]. One solution to this is to use a synthetic antiferromagnet, made up of two ferromagnetic materials separated by a nonmagnetic spacer material (Owing to strong antiferromagnetic coupling effect, Ru is the most popular option [62]). In this stack, the three layers are coupled antiferromagnetically by Ruderman-Kittel-Kasuya-Yosida coupling and by using the optimum thickness of the non-magnetic spacer layer, the antiferromagnet is stabilized reducing the stray fields and asymmetry in the resistance versus field characteristics. Copper is a good candidate for the non-magnetic spacer layer, due to its high conductivity and high interfacial spin dependent scattering [62]. Π-conjugated organic semiconductors have been proposed as spacer materials, due to their relatively strong electron-phonon coupling, large spin coherence and ease of fabrication [63]. However, failure to perform well at room temperature has resulted in relative lack of interest in organic GMR sensors.

GMR sensors are quite attractive as they combine high sensitivity and resolution with low sensor resistance [64]. This lower resistance in turn results in reduced noise levels, higher operational bandwidth and low power consumption for a given sensing current.

4.2. Applications

GMR sensors have a small footprint and are capable of sensing the Earth's magnetic field, which makes them attractive for orientation, navigation and inertial positioning applications. Three GMR sensors packaged orthogonally to each other are used to implement tri-axis magnetometers. In [65], this complex and inconvenient packaging process is avoided by the use of a Ni-Zn ferrite flux guide and 3 in-plane GMR sensors oriented at 120^{o} to create a tri-axis magnetometer (figure 10).

Magnetocardiography (MCG) is a non-invasive contactless method for measuring the activity of the heart using the magnetic fields generated by the electrical impulses that control the operation of the heart. The fields

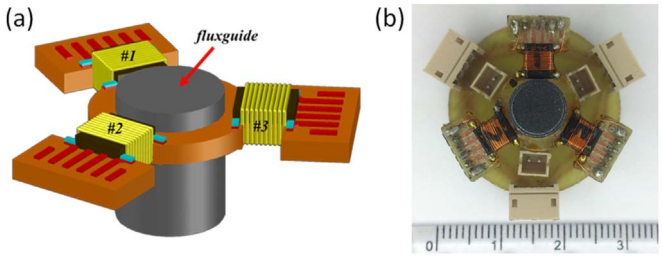

Figure 10. (a) Schematic and (b) photograph of triaxis flux-guide GMR magnetometer. Reproduced with permission from [65] AIP Publishing.

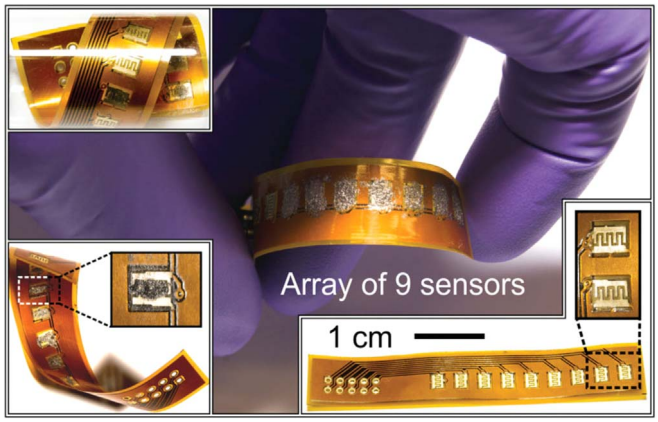

Figure 11. GMR ink painted sensors. Reproduced with permission from [70] John Wiley & Sons. [© 2014 The Authors. Published by WILEY-VCH Verlag GmbH & Co. KGaA, Weinheim].

involved are weak ($\sim 10^{-11}$T) and SQUIDs are the most commonly used MCG sensors. In [66], four liquid He cooled GMR sensors in Wheatstone bridge configuration coupled to a Niobium loop were used as a low power, compact MCG sensor to study the activity of the human heart.

GMR sensors have been used for contactless measurement of current flowing through wires by quantifying the magnetic field induced by the current [67]. Non-destructive contactless evaluation of metal quality in vehicle parts, building structures, etc by eddy current sensing in the presence of an ac magnetic field is another interesting application of GMR sensors [68] with growing potential [11].

In [69], the fabrication of GMR devices on Kapton and Polyester flexible substrates has been reported. The devices were fabricated on the polymer substrates after smoothing the surface by spin coating photoresist on it. These devices had better MR ratio than similar devices fabricated on oxidized Si substrate, owing to a high antiferromagnetic coupling fraction. An interesting approach to fabricating flexible GMR sensors is described in [70]. The process starts with a conventional GMR stack deposition on a rigid substrate pre-coated with a sacrificial layer. The stack is then released and milled to form uniform flakes with an average size of $36 \pm 5\ \mu$m. These flakes are dispersed in polymer bonder to form GMR paste, which can be printed on flexible PCBs to form flexible GMR sensors (figure 11). These sensors exhibit minimal change in GMR ratio and sensitivity with bending radius as low as 1 cm.

Biological specimen detection and quantification using functionalized magnetic nanoparticles, nanowires, etc in conjunction with magnetic sensors is an active area of research. The detection of influenza A virus using GMR sensor and magnetic nanoparticles, with a detection limit of $1.5 \times 102\ \mathrm{TCID}_{50}$/ml (more sensitive than ELISA) has been reported in [71]. In [72], a novel approach to the magnetic particle detection and classification problem is explained, wherein GMR sensors were used to detect E. coli using the difference in velocity between bacteria tagged magnetic microparticles and bare reference superparamagnetic microparticles. In order for the biological specimen to be detected accurately the magnetic beads need to be transported to the vicinity of the GMR sensor. Current based concentrating structures [73] and flow focusing [74] can be used to accomplish this goal. Flow cytometry using GMR sensors shows promise as a low cost alternative to traditional fluorescence cytometry [74]. GMR sensors functionalized with synthetic DNA probes were utilized to detect cancer (melanoma) using circulating tumor DNA (ctDNA) [75]. This liquid biopsy technique is capable of detecting

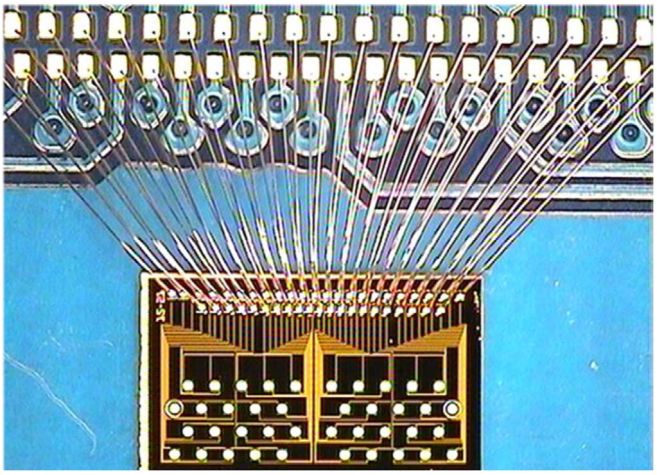

Figure 12. GMR Multi-biomarker Immunoassay for 12 tumor markers. Reproduced from [76] Copyright (2019), with permission from Elsevier.

methylated ctDNA as little as 0.1% of total cell-free DNA, which can enable early detection of cancer. The GMR sensor reported in [76] is capable of multiplex measurement of 12 different tumor markers, which makes it an effective tool in the early detection and therapeutic management of cancers of lung, liver, digestive tract, prostrate, etc (figure 12). The usage of a GMR sensor for real time mercuric ion (Hg^{+2}) detection in drinking water is illustrated in [77]. This system achieves a limit of detection of 10 nM, which is the maximum allowed mercury level in drinking water according to the U.S. Environmental Protection Agency.

5. Tunnel magnetoresistance

5.1. Background

A tunneling magnetoresistance (TMR) sensor consists of two ferromagnetic layers separated by a tunneling barrier; hence also called magnetic tunnel junction (MTJ). The structure is similar to the GMR sensor with the conducting layer being replaced by an insulator (figure 13). When two ferromagnets are magnetized in parallel direction, there is higher probability of the electrons to tunnel through the insulation layer than if the magnetizations of the two layers were antiparallel. Thus, the parallel configuration results in minimum resistance and the antiparallel configuration results in maximum resistance. Julliere first observed spin dependent quantum tunneling in magnetic tunnel junctions comprised of Fe and Co layers separated by an amorphous Ge layer [78].

In a typical TMR sensor, one of the ferromagnetic layers is free to rotate with the applied field, while the magnetization of the other layer is pinned. Similar to the GMR sensors, empirically it can be shown that the resistance of the TMR stack is proportional to the cosine of the angle between the free and the pinned layer (equation (8)). Thus, in order to fabricate a TMR sensor with linear response to an applied magnetic field, it is imperative that the reference layer magnetization be pinned perpendicular to the free layer (equation (9)).

Similar to the GMR sensor, the two ferromagnetic layers are made using soft ferromagnetic alloys such as NiFe, CoFe, CoFeB, etc The reference layer magnetization is pinned by contact with either a natural antiferromagnet such as IrMn or a synthetic antiferromagnet as detailed in [61]. Due to the ease of deposition in a pinhole-free well-adhered manner, amorphous aluminum oxide was a popular choice for the tunneling barrier [79], and it resulted in devices with magnetoresistance of few 10%. The prevalence of large tunnel magnetoresistance (>1000%) in TMR devices using epitaxially grown crystalline MgO as the tunnel barrier was predicted in [80, 81]. The crystalline nature of MgO allows for coherent tunneling of Δ_1 Bloch states from either side of the tunneling layer, which results in higher magnetoresistance than aluminum oxide-based TMR sensors [82]. This prediction spurred on research in MgO crystalline tunneling barriers in MTJs, culminating in the development of devices with extremely high room temperature magnetoresistance (e.g. 604%, [83, 84]).

TMR sensors are more sensitive than GMR sensors. However, they suffer from higher noise. They have higher resistance and thereby consume lesser power than a GMR sensor at the same operating voltage. Also, TMR sensors are more expensive and difficult to fabricate, due the need for a high quality, pinhole free extremely thin tunneling barrier. GMR sensor fabrication can be simplified by using in plane contacts, since the change in resistance is observed for conduction through the three layers as well as along them. TMR sensor cannot use in-

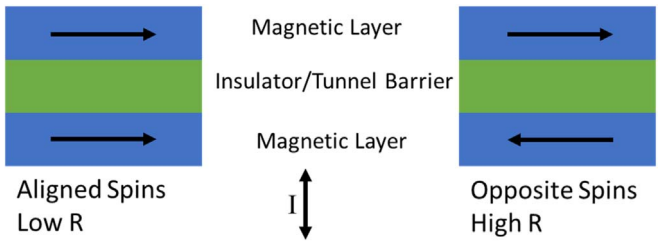

Figure 13. Tunnel Magnetoresistance sensor schematic showing the allowed directions of current through the sensor.

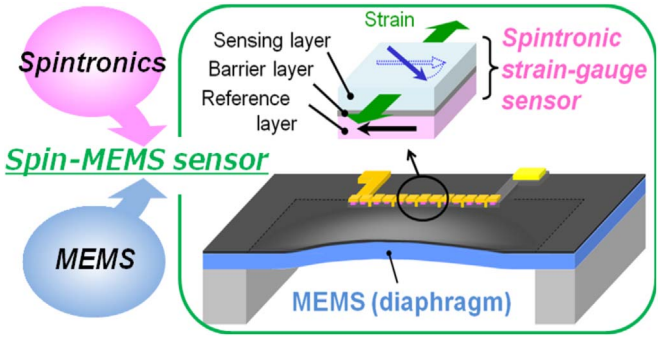

Figure 14. The melding of spintronics and MEMS created the high sensitivity Spin-MEMS strain gauge and microphone schematic. Reproduced with permission from [92] © [2017] IEEE.

plane contacts, as the spin dependent scattering of tunneling electrons only occurs for electrons flowing through the tunneling barrier either from top to bottom or vice-versa.

5.2. Applications

Due to their high sensitivity, MTJs are an attractive option for contactless current measurement. In [85] an MTJ-based current sensing system with sensitivity of 7.74 mV A^{-1} targeting smart grid systems is reported. MTJ devices have been incorporated in conventional CMOS ICs to monitor current flow at the microscale with a sensitivity of 1.6 mV/V/mA, as shown in [86].

The resistance of a TMR device in the anti-parallel state is sensitive to temperature, due to spin-wave excitation. The response time of such a device is faster than conventional CMOS thermal sensor, which relies on electron diffusion. Two TMR sensors were used to make an on-chip compensated temperature sensor for temperature monitoring and IC overheat protection [87]. In [88], the temperature dependence of stochastic TMR switching is exploited to make a temperature biased random number generator that consumes 1–2 orders of magnitude lower energy than state-of-the-art CMOS sensors.

An array of 10 TMR sensors connected in series is used to detect metal cracks as shallow as 200 μm in an aluminum specimen, with a signal-to-noise-ratio (SNR) of approximately 34 dB, using eddy current sensing [89]. An improved version of this system with 28 series connected TMR sensors demonstrated the ability to sense aluminum defects as shallow as 100 μm with 115 dB SNR [90]. It was shown that while the sensitivity of the system increases with the number of TMR sensors connected in series, the resistance and noise also increases, thereby an array of 28 TMRs delivered better resolution than a 52 TMR sensor array [90].

By utilizing a magnetostrictive material as the free layer in a TMR sensor, strain acting on the TMR gets converted to a magnetic field which causes a change in the sensor resistance. In [91], magnetostrictive $Co_{40}Fe_{40}B_{20}$ free layer is used in an MgO barrier based TMR sensor to fabricate a strain gauge with a gauge factor of 2150 $\pm$ 30 under an applied bias field of -3.2 kA m^{-1}. The strain gauge design was further improved in [92] by using an amorphous Fe-B free layer, which results in a gauge factor of 5072, at an applied bias field of 1.2 kA/m (figure 14). In this work it was also demonstrated, that by fabricating the amorphous Fe-B TMR on a diaphragm, a SpinMEMS microphone of 57 dB(A) gain can be realized. TMR based strain gauges offer large gauge factors (~25 times larger than state of the art Si piezoresistor strain gauges), however the need for a uniform biasing magnetic field for proper strain gauge operation is a daunting requirement for most applications.

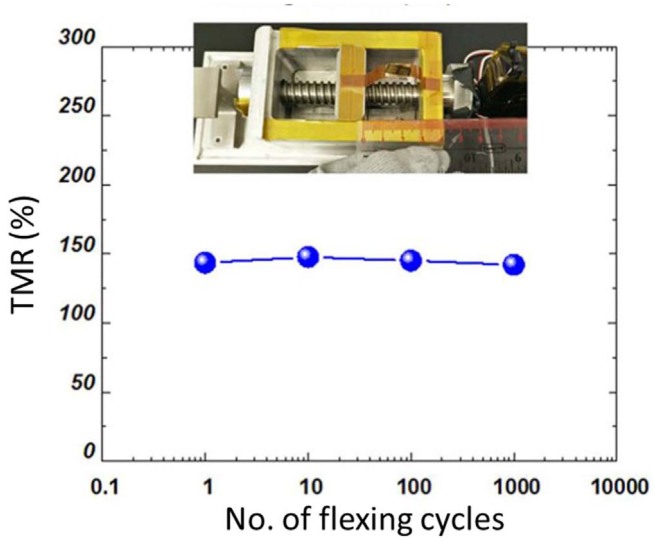

Figure 15. Flexing cycle invariant operation exhibited by flexible TMR sensor. Inset depicts flexing setup. Reproduced with permission from [98] John Wiley & Sons. [© 2018 WILEY-VCH Verlag GmbH & Co. KGaA, Weinheim].

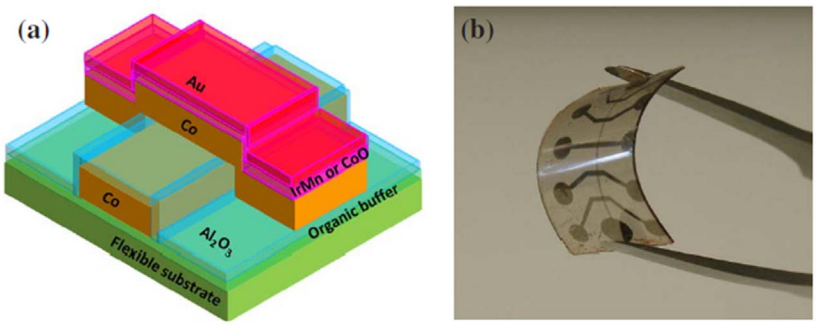

Figure 16. TMR sensor fabricated on flexible organic substrate: (a) schematic and (b) fabricated sensor. Reproduced from [99] with the permission of AIP Publishing..

The average resistance of a TMR device varies, when it is subjected to a microwave magnetic field. This phenomenon is exploited in [93] to develop an on-chip microwave phase and spectrum analyzer. Far field microwave radiation is rectified by TMRs using the Seebeck effect with an efficiency of 1–10 mV mW^{-1} [94]. This technique was successfully used to detect hidden objects as small as few wavelengths in the microwave regime (~few cm).

Conventionally, magnetoresistance read heads are used in high density magnetic storage media (such as hard drives). In [95], the usage of TMR to read magnetic ink patterns for security and industrial applications is demonstrated. The TMR sensor based scanning microscope was shown to have spatial resolution better than 7 μm, when used to image remanent magnetic fields [96].

In [97], the use of substrate thinning to achieve a thin and flexible TMR sensor capable of operating reliably down to a bending radius as small as 5 mm and 1000 flexing cycles is demonstrated. The TMR device is fabricated using conventional processes on a Si substrate. Subsequently, the thickness of the substrate is reduced from 500 μm to 14 μm by deep reactive ion etching from the back to impart flexibility. In [98], this process is improved upon further by reducing the Si substrate thickness to 5 μm. The resulting TMR device exhibits enhanced flexibility and is capable of being bent to an astonishingly small radius of 0.5 mm and can work well beyond 1000 flexing cycles (figure 15). This flexible TMR sensor has been mounted on tip of cardiac catheter to guide its motion through the blood vessels.

A flexible MTJs fabricated on a buffered organic substrate is demonstrated in [99]. A commercially available Gel-film® flexible sheet serves as the substrate. The substrate surface is smoothened by coating with photoresist and poly [3,4-ethylenedioxythiophene)poly(styrenesulfonate) (PEDOT-PSS) (figure 16). This device is capable of functioning down to a bending radius of 15 mm.

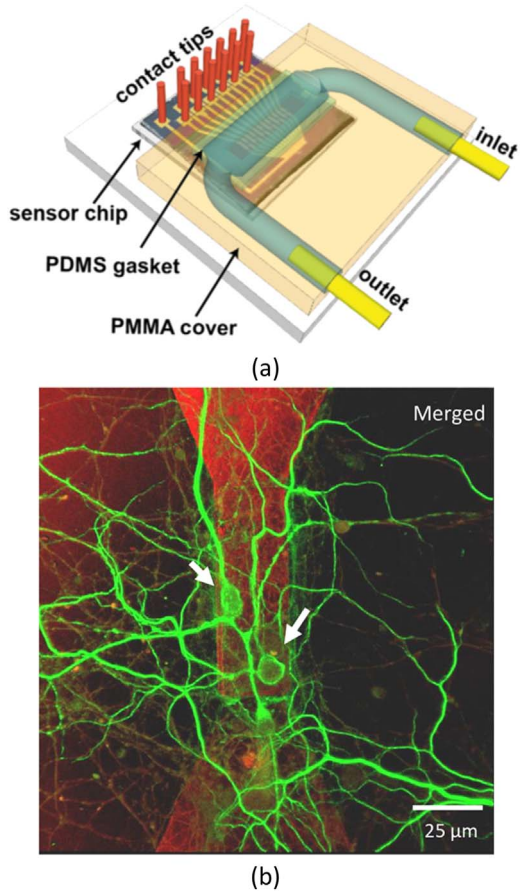

Figure 17. (a) Integrated TMR microfluidic system for detecting pathogenic DNA. Reproduced with permission from [101] Copyright (2017), with permission from Elsevier (b) Rat hippocampal neurons cultured atop capped TMR sensor (merged MAP-2 and Tau stain). Reproduced with permission from [104], © 2018 Daniela Moretti *et al.*

Owing to their small size, large sensitivity and relative ease of measurement, TMR sensors are attractive for different biological applications. In [100], the detection of alpha-fetoprotein(AFP), which is an important hepatic tumor marker in concentrations down to 0.002 mg/ml using 20 nm superparamagnetic iron nanoparticles and MgO-based TMR sensors in sandwich assay configuration is presented. The detection of pathogen DNA from hepatitis-E virus and listeria and salmonella bacteria using TMR sensors and magnetic nanoparticles with sub-nM range sensitivity is presented in [101] (figure 17(a)). The commonly used magnetic biosensor concept employs a functionalization layer on top of the sensor surface to trap target moieties (bacteria, viruses, DNA, etc). This has been modified by using a mechanical trap [102] and later an electromechanical trap [103], omitting the need for a functionalization layer and simplifying the detection process by reducing the work steps. TMR sensors were used for in-vitro sensing of neuronal networks in [104] (figure 17(b)). Biocompatibility and viable neuron culture on TMR sensors were achieved by capping the TMR device with SiO_2(50 nm)/Si_3N_4(25 nm)/SiO_2(50 nm) layer.

6. Giant magnetoimpedance

6.1. Background

The large impedance change of an alternating current powered ferromagnetic conductor upon the change of a magnetic field is referred as Giant Magnetoimpedance (GMI) effect. The complex impedance is determined by the skin effect in conjunction with the complex magnetic permeability. Detailed studies by Charles Kittle in 1946 on the characteristics of soft magnetic material's permeability at high frequency was one of the early works that revealed the theoretical basis of this classical electromagnetic phenomena [89]. In 1993, through large impedance change observed in amorphous wire by Larissa V. Panina and Kaneo Mohri, GMI was identified as a sensing effect for the first time, and has since attracted strong interest due to its high magnetic sensitivity, achieved with simple fabrication process and relatively low cost.

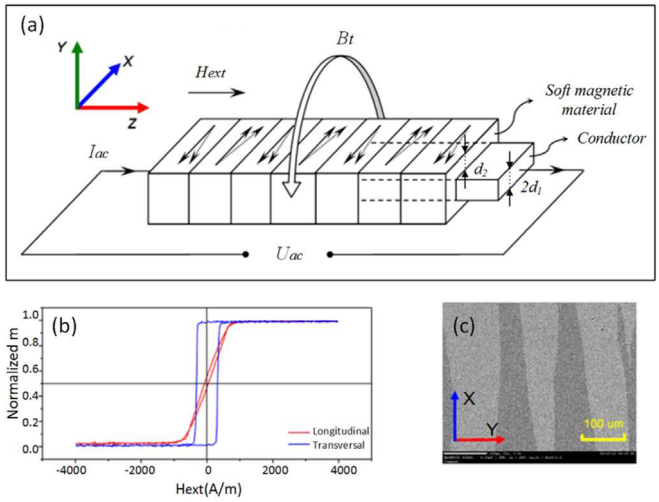

Figure 18. (a) Schematic view of a multilayer thin film GMI sensor. An alternating current, $I_{ac,}$ is applied in longitudinal direction, which induces transverse magnetic flux B_t through interactions with the neighboring magnetic layers. Upon application of an external magnetic field H_{ext}, the magnetization rotates into the direction of H_{ext} (dotted arrows), resulting in the change of permeability, skin depth, and impedance of the device (b) Magnetization curves obtained by vibrating sample magnetometry of a magnetic thin film in transversal and longitudinal directions, revealing the transverse anisotropy in the soft magnetic layers. (c) Domain pattern of the magnetic layer, which confirms the well-defined transverse anisotropy.

The skin effect of a magnetic conducting material is characterized by the penetration depth, given by

$$\delta = 1/\sqrt{\pi f \sigma \mu} \tag{10}$$

where f is the frequency of the alternating current, σ and μ are electrical conductivity and magnetic permeability respectively.

The impedance model of a magnetic wire can be derived from Maxwell equations, expressed as

$$Z = R_{dc} kr \xi_0(kr) / 2\xi_1(kr) \tag{11}$$

where

$$k = (1 + j)/\delta \tag{12}$$

R_{dc} is the dc resistance of the wire, ξ_0, ξ_1 are the Bessel functions, r is the radius of the wire, j is the imaginary unit. The analytical model of the GMI wire is obtained through simplifications of the geometry. The approach generally applies to GMI devices of uni-body soft magnetic materials. A similar expression can be obtained for soft magnetic material of single layer planar structure [105].

Since the introduction of the GMI amorphous wire, GMI sensors in ribbons [106], multilayer thin films [107], and multilayer thin films with complex planar geometries [108] were developed, each showing unique advantages in different applications.

The maximum relative impedance change of a GMI device is defined as GMI ratio, given by

$$GMI = \frac{Z(H) - Z(H_{\max})}{Z(H_{\max})} \tag{13}$$

where $Z(H_{max})$ is the impedance at saturation magnetic field, when its relative permeability is close to 1, resulting in a minimal impedance value $Z_{min} = Z(H_{max})$ as a benchmark. GMI ratio is a simply way to experimentally characterize the device for performance evaluation. GMI ratios up to 800% were reported in GMI devices with different configurations [109].

Although GMI sensors share similar impedance characteristics under applied magnetic field, the major contributors to the impedance change vary upon the device configurations, geometries, and operating frequencies. This is due to the fact that skin effect only plays a major role in the impedance change when the penetration depth reaches the order of the thickness of the magnetic material. For typical GMI wires and ribbons, whose thicknesses are in the order of tens of micrometers, large impedance change in associated with skin effect can be achieved in the frequency range of kHz to MHz. For thin film based GMI sensors with film thickness in the order of hundreds of nanometers, the corresponding frequency for effective skin effect is in gigahertz range. The high frequency not only introduces complexity to the measurement circuit, but also pushes the magnetization behavior into the ferromagnetic resonance regime, which could result in flattened GMI characteristic curves [110].

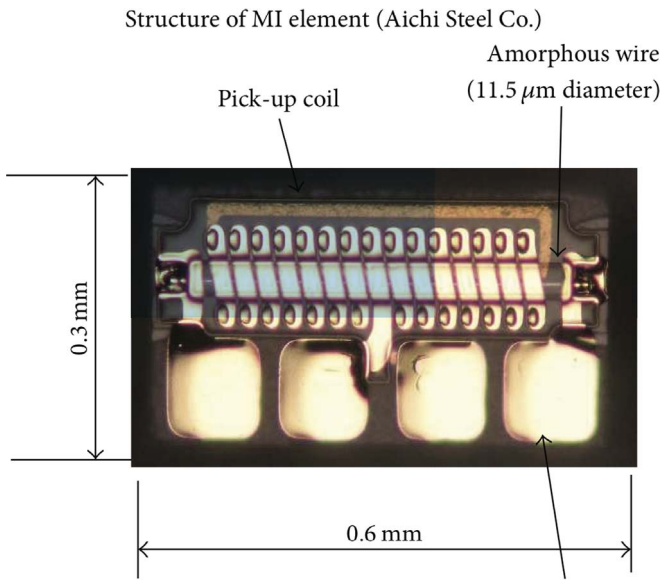

Figure 19. Mass production type amorphous wire MI element fabricated by Aichi Steel Co. Reproduced with permission from [118]. © 2015 Kaneo Mohri *et al*.

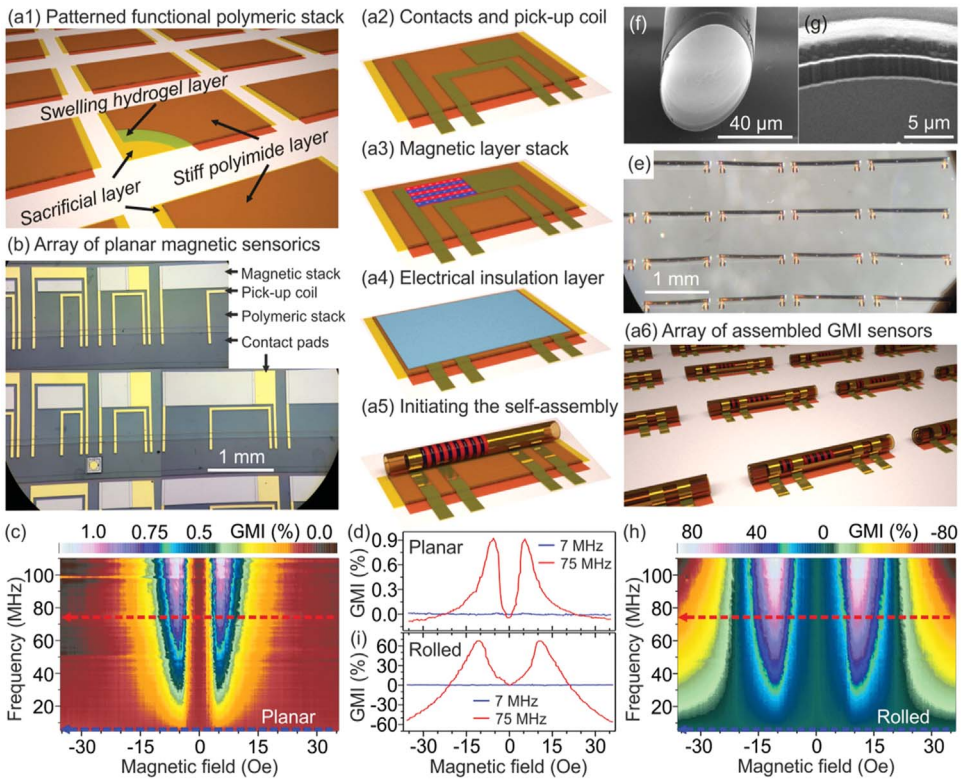

Figure 20. Fabrication and characterization of on-chip-integrated GMI sensorics: (a) Schematics of the fabrication steps to realize arrays of tubular GMI sensor elements. Optical micrograph of an array of (b) planar and (e) self-assembled device. 3D map of the GMI response versus frequency and magnetic field measured of the c) planar and h) self-assembled device. Magnetic field dependences of the GMI response of (d) planar and (i) self-assembled structure. (f) SEM image of the tube edge. (g) FIB cut through the tube revealing 2 windings firmly attached to each other without forming voids. Reproduced with permission from [122] on from [103] John Wiley & Sons. [© 2015 The Authors. Published by WILEY-VCH Verlag GmbH & Co. KGaA, Weinheim].

To achieve optimal GMI effect with moderate frequencies, GMI thin film sensors are developed with a conducting layer sandwiched by soft magnetic layers, as shown in figure 18(a). The conducting layer offers a large dynamic range of conductivity, whereas the soft magnetic layers are responsible for providing a dynamic permeability through magnetization interactions with external magnetic field.

The analytical model of the impedance for a magnetic/conducting/magnetic tri-layer structure is given by [111]

$$Z = R_{\mathrm{dc}}\left(1 - 2j\mu\frac{d_1 d_2}{\delta_c^2}\right) \tag{14}$$

where R_{dc} is the dc resistance of the inner conductor, $2d_1$ is the thickness of the conductor, d_2 is the thickness of the magnetic layers as shown in figure 18(a), δ_c is the skin depth of the conducting layer, the permeability of the magnetic layer $\mu = \mu(f, H_{ext})$ is a function of the frequency f and external magnetic field H_{ext}.

Regardless of structural variations, being magnetically soft and with well-defined magnetic anisotropies are the two key enablers for GMI materials of superior performances [112, 113]. Magnetostrictive Co-based and Fe-based amorphous magnetic alloys were used in fabrication of GMI wires and ribbons. The circumferential and transverse magnetic anisotropies are established through fabrication-induced stresses. As a comparison, thin film GMI sensors benefit from standard microfabrication process, and rely on field deposition or field annealing to establish preferred transverse anisotropy (figures 18(b), (c)). Permalloy ($Ni_{0.81}Fe_{0.19}$) is commonly used as material as it provides high permeability and zero magnetostriction.

6.2. Applications

As early as Qin dynasty in ancient China, compass was invented for navigation, aligning building directions and fortune telling, which marked the successful implementations of the most primitive magnetic sensors. In modern society, magnetic sensors are implemented in a large number of applications including geographic navigation, metal detection, drug delivery, data storage, to name a few, and are employed in different fields like automotive, biomedical or consumer electronics. As a member of magnetic sensor family, GMI sensor is the only ac-based magnetic sensor, which operates in a wide range of frequencies from kHz to GHz, providing a large impedance change under the applied magnetic field. For this reason, GMI sensors have been explored and integrated in a RF system as a passive wireless magnetic sensor [114]. In terms of detectable field range, GMI sensor covers a wide range of magnetic fields from geomagnetic to biomagnetic, significantly more sensitive than Hall effect sensor, superior than MR sensors (GMR, TMR), comparable to flux gate, and several orders less sensitive than SQUID (superconducting quantum interference device). When it comes to the sensor size, GMI element is typically sized from several millimeters to sub-millimeter as compared to the micrometer MR sensors, although it's larger, it does not make a big difference via typical SMD (surface mounting device) packaging in most commercial electronic applications.

Amorphous wire GMI sensor was first commercialized and mass-produced by Aichi Steel Co. Japan in 2005. The GMI wire was excited by a pulse generation circuit, a MEMS pickup coil is fabricated around the GMI element to generate linear output voltage through electromagnetic induction (figure 19). Based on this design, 3-axis GMI sensors with magnetic field resolution of 160 nT were developed and utilized in consumer electronic device such as smart phones and smart watches and industrial applications. In addition, highly sensitive GMI sensors with magnetic field resolution of around 1 pT were also commercialized for biomagnetic applications such as for an in vitro biopsy fragment of guinea-pig stomach [115], the human magneto-cardiogram, the human back magnetocardiogram, and the human magneto-encephalogram [116–118].

Despite the success of the commercialization of the amorphous wire GMI sensors, the thin film multilayer has been a popular GMI configuration in the research domain over the past decades thanks to its promising performance and standard microfabrication manufacturing process [119, 120]. The physical vapor deposition based microfabrication method enables easy fabrication and integration of thin film GMI sensor in various unique systems such as with flexible substrate [121], MEMS (figure 20) [122], surface acoustic wave devices [112], microfluidic devices [123], nanowires [124], etc.

7. Discussion and summary

In this paper, different magnetic solid-state magnetic field sensors were reviewed. The underlying physics and the different device structures used to exploit and enhance the conversion of the magnetic field into electrically measurable signals were discussed.

Figure 21 shows a comparison of the detectable field range, sensor size and operating mode of the conventional magnetic sensors. Interestingly, as far as sensors reported in literature go, the sensitivity is highest for GMI sensors, which commercially play a minor role. They are followed by TMR sensors with AMR, GMR and Hall sensors bringing up the rear (table 1). When it comes to commercially available sensors, the analog front end and the associated processing circuitry become important factors influencing the performance of the sensor. It also has a major impact on the power consumption, when comparing commercial solutions with their research counterparts. In table 1, commercial analog magnetic sensors [125–132] are compared. However, with

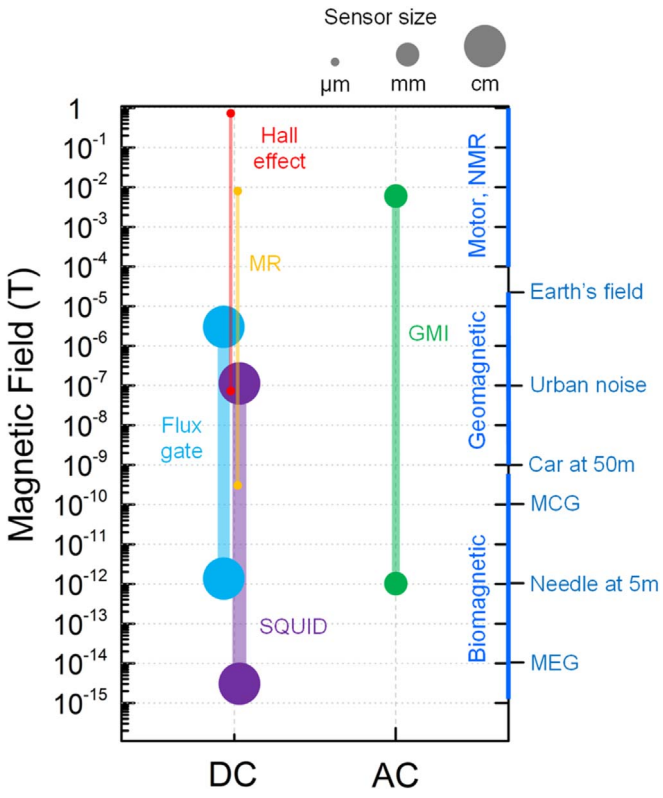

Figure 21. Comparison of the measurement range of magnetic field sensors.

the shift in industry towards application specific sensors (such as position sensors, current sensors, etc) and sensors with digital readout, the parameters listed in the table may not be indicative of the best performance that can be obtained using a particular sensor technology. Among the MR sensors, TMR sensors end up performing the best. Not surprisingly, the TMR sensor is also the most expensive one. GMR sensors perform better than AMR sensors. Hall sensors have the least sensitivity and resolution; however, they make up for it by offering a high dynamic range at low cost. The low cost, adequate performance and high availability makes Hall effect sensor the most popular magnetic field sensor on the market [7]. The best performance is offered by the GMI sensors, however this comes at the expense of a large footprint. While all the other sensors reported in the table are single IC sensors, the GMI sensors consist of multiple discrete components on a PCB [130, 131], which may not be amenable to certain applications.

With the advent of the internet of things and the plethora of opportunities for applications relying on continuous magnetic field monitoring in various fields such as industrial electronics, medical diagnostics, point of care, remote monitoring, there has been a need for flexible, conformal and compact sensors. Different approaches to achieving thin and flexible magnetic sensors were presented and it was observed that buffered polymer substrate-based sensors offer good performance (comparable to their rigid counterparts) and also the potential for low cost manufacturing due to reduced substrate costs.

The use of magnetic sensing for medical applications presents an area of opportunity, growth and expansion for the magnetic sensor industry. Magnetic sensing systems have been demonstrated for different applications such as tumor detection, pathogen DNA detection, neuronal network sensing, drinking water contaminant detection, magnetic encephalograms, etc However, the need of the hour is to rigorously test and subject the plethora of magnetic biomedical sensors discussed in research articles to clinical trials and bring them from the lab to the market. This will have wide-ranging impact on the cost and delivery of preventive, diagnostic and curative healthcare.

Numerous phenomena have been exploited over the years to develop magnetic field sensing devices. Currently, all sensing methods used for magnetic measurements are relatively mature. Improved materials and better electronics are delivering incremental improvements in performance, size and power consumption. The demand for higher sensitivity in industrial applications will most likely lead to a partial replacement of Hall effect sensors by GMR or TMR sensors, which in turn will have to become more affordable. The performance increase of printing technologies, especially in terms of resolution, is a promising development from which innovation in the areas of sensor fabrication and integration can be

Table 1. Comparison of different sensors.

	Sensor	Sensitivity	Resolution (nT/$\sqrt{\text{Hz}}$)	Power (mW)	Bandwidth (kHz)	Cost (US$)
Research	Hall (graphene [23])	5700 V/AT	50	–	3	–
	AMR [38]	4200 ppm/Oe	150	0.4545	–	–
	GMR [64]	6800 ppm/Oe	2.7	–	100	–
	TMR [84]	33000 ppm/Oe	0.95	0.089	100	–
	GMI [120]	550000 ppm/Oe	0.122	–	–	–
Commercial	Hall (Allegro A1324)[126]	5 mV/Oe	130	35	17	2.2
	Hall (Allegro A1325)[126]	3.125 mV/Oe	130	35	17	2.2
	Hall (Allegro A1326)[126]	2.5 mV/Oe	130	35	17	2.2
	AMR (HMC -1002) [127]	16 mV/Oe	2.7	–	5000	34
	AMR (KMX 2X S) [128]	1.87 mV/Oe	–	45	–	8.71
	AMR (HMC -1043L) [129]	5 mV/Oe	–	25	5000	–
	GMR (AAH002-02E) [125]	72.5 mV/Oe	–	100	75	13.85
	GMR (AAH004-00) [125]	4 mV/Oe	–	N/A	–	6.65
	GMR (AA002-02) [125]	3.6 mV/Oe	–	N/A	–	9.6
	TMR (STJ-240) [130]	120 mV/Oe	5	14.4	5000	50
	GMI (MI-CB-1DM) [131]	400 mV/Oe	15		10	–
	GMI (MI-CB-1DH) [132]	100000 mV/Oe	0.001	75	1	–

expected in the future. Discovery of newer transduction methods, materials and device structures can further push magnetic field sensing into a new paradigm.

ORCID iDs

Mohammed Asadullah Khan https://orcid.org/0000-0002-4219-2149
Jian Sun https://orcid.org/0000-0002-7992-8092

References

[1] Barber G and Arrott A 1988 History and magnetics of compass adjusting *IEEE Trans. Magn.* **24** 2883–5
[2] Bray H 2014 *You Are Here: From the Compass to GPS, the History and Future of How We Find Ourselves* (Basic Books)
[3] Caneva K L 1980 Ampère, the etherians, and the Oersted connexion *The British Journal for the History of Science.* **13** 121–38
[4] Faraday M 2016 *Experimental Researches In Electricity* (Read Books Ltd)
[5] Maxwell J C 1881 *A Treatise on Electricity and Magnetism* (Clarendon press)
[6] Ørsted H C 2014 *Selected Scientific Works of Hans Christian Ørsted* (Princeton, NJ: Princeton University Press)
[7] Yd C 2017 *Magnetic Sensor Market and Technologies: Yole Développement*
[8] Lenz J and Edelstein S 2006 Magnetic sensors and their applications *IEEE Sensors J.* **6** 631–49
[9] Weinstock H 2012 *SQUID Sensors: Fundamentals, Fabrication and Applications* (Springer Science & Business Media)
[10] Leahy R 2018 *Advances in Micro-SQUID Design Could Detect And Manipulate Single Electrons.* (AIP Publishing) (https://doi.org/10.1063/1.5044741)
[11] Zheng C *et al* 2019 *Magnetoresistive Sensor Development Roadmap (Non-Recording Applications).* 55 (IEEE Transactions on Magnetics) 1–30
[12] Das KG R and He X 2018 *Flexible, Printed and Organic Electronics 2019–2029: Forecasts, Players & Opportunities* (IDTechEx)
[13] Hall E 1880 On a new action of the magnet on electric currents *Am. J. Sci.* **111** 200–5
[14] Ramsden E 2011 *Hall-Effect Sensors: Theory And Application* (Amsterdam: Elsevier)
[15] Blagojevic M, Kayal M, Gervais M and De Venuto D 2006 SOI Hall-sensor front end for energy measurement *IEEE Sensors J.* **6** 1016–21
[16] Paun M-A 2015 Three-dimensional simulations in optimal performance trial between two types of Hall sensors fabrication technologies *J. Magn. Magn. Mater.* **391** 122–8
[17] Sadeghi M, Sexton J, Liang C-W and Missous M 2015 Highly sensitive nanotesla quantum-well Hall-effect integrated circuit using GaAs–InGaAs–AlGaAs 2DEG *IEEE Sensors J.* **15** 1817–24
[18] Haned N and Missous M 2003 Nano-tesla magnetic field magnetometry using an InGaAs–AlGaAs–GaAs 2DEG Hall sensor *Sens. Actuators, A* **102** 216–22
[19] Xu H *et al* 2013 Batch-fabricated high-performance graphene Hall elements *Sci. Rep.* **3** 1207
[20] Izci D, Dale C, Keegan N and Hedley J 2018 The construction of a graphene hall effect magnetometer *IEEE Sensors J.* **18** 9534–41
[21] Joo M-K, Kim J, Lee G, Kim H, Lee Y H and Suh D 2017 Feasibility of ultra-sensitive 2D layered Hall elements *2D Mater.* **4** 021029
[22] Huang L, Zhang Z, Chen B, Ma X, Zhong H and Peng L-M 2014 Ultra-sensitive graphene Hall elements *Appl. Phys. Lett.* **104** 183106
[23] Dauber J *et al* 2015 Ultra-sensitive Hall sensors based on graphene encapsulated in hexagonal boron nitride *Appl. Phys. Lett.* **106** 193501
[24] Wang Z, Shaygan M, Otto M, Schall D and Neumaier D 2016 Flexible Hall sensors based on graphene *Nanoscale.* **8** 7683–7
[25] Lin G, Makarov D and Schmidt O G 2017 Magnetic sensing platform technologies for biomedical applications *Lab Chip* **17** 1884–912
[26] Liu P, Skucha K, Megens M and Boser B A 2011 CMOS Hall-effect sensor for the characterization and detection of magnetic nanoparticles for biomedical applications *IEEE Trans. Magn.* **47** 3449–51
[27] Issadore D *et al* 2012 Ultrasensitive clinical enumeration of rare cells *ex vivo* using a micro-hall detector *Sci. Transl. Med.* **4** 141ra92
[28] Sekino M *et al* 2018 Handheld magnetic probe with permanent magnet and Hall sensor for identifying sentinel lymph nodes in breast cancer patients *Sci. Rep.* **8** 1195
[29] Schrittwieser S *et al* 2016 Homogeneous biosensing based on magnetic particle labels *Sensors* **16** 828
[30] Giouroudi I and Hristoforou E 2018 Perspective: magnetoresistive sensors for biomedicine *J. Appl. Phys.* **124** 030902
[31] Granell P N *et al* 2019 Highly compliant planar Hall effect sensor with sub 200 nT sensitivity *NPJ Flexible Electronics.* **3** 3
[32] Melzer M *et al* 2015 Wearable magnetic field sensors for flexible electronics *Adv. Mater.* **27** 1274–80
[33] Satake Y, Fujiwara K, Shiogai J, Seki T and Tsukazaki A 2019 Fe-Sn nanocrystalline films for flexible magnetic sensors with high thermal stability *Sci. Rep.* **9** 3282
[34] Heidari H, Bonizzoni E, Gatti U, Maloberti F and Dahiya R 2016 CMOS vertical Hall magnetic sensors on flexible substrate *IEEE Sensors J.* **16** 8736–43
[35] Huang L *et al* (ed) 2015 Flexible graphene hall sensors with high sensitivity *2015 IEEE Int. Electron Devices Meeting (IEDM)* (Piscataway, NJ: IEEE)
[36] Thomson W X I X 1857 On the electro-dynamic qualities of metals:-Effects of magnetization on the electric conductivity of nickel and of iron *Proc. R. Soc. Lond.* **8** 546–50
[37] Popovic R, Flanagan J and Besse P 1996 The future of magnetic sensors *Sens. Actuators, A* **56** 39–55
[38] Wang Z *et al* 2016 Highly sensitive flexible magnetic sensor based on anisotropic magnetoresistance effect *Adv. Mater.* **28** 9370–7
[39] Akhter M, Mapps D, Ma Tan Y, Petford-Long A and Doole R 1997 Thickness and grain-size dependence of the coercivity in permalloy thin films *J. Appl. Phys.* **81** 4122–4
[40] Freitas P *et al* 2004 Magnetoresistive DNA chips *Magnetoelectronics* (Amsterdam: Elsevier) pp 331–86
[41] Grosz A, Mor V, Amrusi S, Faivinov I, Paperno E and Klein L 2016 A high-resolution planar Hall effect magnetometer for ultra-low frequencies *IEEE Sensors J.* **16** 3224–30
[42] Grosz A *et al* 2013 Planar hall effect sensors with subnanotesla resolution. *IEEE Magn. Lett.* **4** 6500104
[43] König F and Müller J (ed) 2010 A novel micro paramagnetic oxygen sensor based on an anisotropic magneto resistance-device *Sensors* (IEEE) 2010: IEEE

[44] Dimitrova P, Andreev S and Popova L 2008 Thin film integrated AMR sensor for linear position measurements *Sens. Actuators, A* **147** 387–90
[45] Tumanski S 2001 *Thin Film Magnetoresistive Sensors* (Boca Raton, FL: CRC Press)
[46] Yu P *et al* (ed) Development of a compliant magnetic 3D tactile sensor with AMR elements *Int. Conf. on Intelligent Robotics and Applications*2014*(Berlin)* (Springer)
[47] Lai W-M *et al* (ed) 2015 Monolithic integration of micro magnetic pillar array with anisotropic magneto-resistive (AMR) structure for out-of-plane magnetic field detection *Micro Electro Mechanical Systems (MEMS), 2015 28th IEEE Int. Conf. on (Piscataway, NJ)* (IEEE)
[48] Guo Y, Deng Y and Wang S X 2017 Multilayer anisotropic magnetoresistive angle sensor *Sens. Actuators, A* **263** 159–65
[49] Verpillat F *et al* 2008 Remote detection of nuclear magnetic resonance with an anisotropic magnetoresistive sensor *Proc. Natl Acad. Sci.* **105** 2271–3
[50] He D, Shiwa M, Jia J, Takatsubo J and Moriya S 2011 Multi-frequency ECT with AMR sensor *NDT & E International.* **44** 438–41
[51] Griesbach T, Wurz M C and Rissing L 2012 Design, fabrication, and testing of a modular magnetic field microsensor on a flexible polymer foil *IEEE Trans. Magn.* **48** 3843–6
[52] Choe G and Steinback M 1999 Surface roughness effects on magnetoresistive and magnetic properties of NiFe thin films *J. Appl. Phys.* **85** 5777–9
[53] Akin M, Pratt A, Blackburn J and Dietzel A 2018 Based magneto-resistive sensor: modeling, fabrication *Characterization, And Application. Sensors.* **18** 4392
[54] Jiang Z, Llandro J, Mitrelias T and Bland J 2006 An integrated microfluidic cell for detection, manipulation, and sorting of single micron-sized magnetic beads *J. Appl. Phys.* **99** 08S105
[55] Donolato M *et al* 2009 Nanosized corners for trapping and detecting magnetic nanoparticles *Nanotechnology* **20** 385501
[56] Hien L, Quynh L *et al* 2016 DNA-magnetic bead detection using disposable cards and the anisotropic magnetoresistive sensor *Adv. Nat. Sci.: Nanosci. Nanotechnol.* **7** 045006
[57] Binasch G, Grünberg P, Saurenbach F and Zinn W 1989 Enhanced magnetoresistance in layered magnetic structures with antiferromagnetic interlayer exchange *Physical Review B.* **39** 4828
[58] Baibich M N *et al* 1988 Giant magnetoresistance of (001) Fe/(001) Cr magnetic superlattices *Phys. Rev. Lett.* **61** 2472
[59] Dieny B, Speriosu V S, Parkin S S, Gurney B A, Wilhoit D R and Mauri D 1991 Giant magnetoresistive in soft ferromagnetic multilayers *Physical Review B.* **43** 1297
[60] Heim D, Fontana R, Tsang C, Speriosu V, Gurney B and Williams M 1994 Design and operation of spin valve sensors *IEEE Trans. Magn.* **30** 316–21
[61] Bandiera S *et al* 2010 Comparison of synthetic antiferromagnets and hard ferromagnets as reference layer in magnetic tunnel junctions with perpendicular magnetic anisotropy *IEEE Magn. Lett.* **1** 3000204
[62] Wang S X and Li G 2008 Advances in giant magnetoresistance biosensors with magnetic nanoparticle tags: review and outlook *IEEE Trans. Magn.* **44** 1687–702
[63] Xiong Z, Wu D, Vardeny Z V and Shi J 2004 Giant magnetoresistance in organic spin-valves *Nature* **427** 821
[64] Guedes A *et al* 2012 Towards picoTesla magnetic field detection using a GMR-MEMS hybrid device *IEEE Trans. Magn.* **48** 4115–8
[65] Chiang C-Y, Jeng J-T, Lai B-L, Luong V S and Lu C-C 2015 Tri-axis magnetometer with in-plane giant magnetoresistance sensors for compass application *J. Appl. Phys.* **117** 17A321
[66] Pannetier-Lecoeur M, Parkkonen L, Sergeeva-Chollet N, Polovy H, Fermon C and Fowley C 2011 Magnetocardiography with sensors based on giant magnetoresistance *Appl. Phys. Lett.* **98** 153705
[67] Ouyang Y, He J, Hu J and Wang S X 2012 A current sensor based on the giant magnetoresistance effect: design and potential smart grid applications *Sensors* **12** 15520–41
[68] Mareschal O, Cordier C, Dolabdjian C and Finkel P 2018 Aluminum alloy sensitization evaluation by using eddy current techniques based on igmr-magnetometer head *IEEE Trans. Magn* **55** 6200104
[69] Yf C *et al* 2008 Towards flexible magnetoelectronics: buffer-enhanced and mechanically tunable GMR of Co/Cu multilayers on plastic substrates *Adv. Mater.* **20** 3224–8
[70] Karnaushenko D, Makarov D, Stöber M, Karnaushenko D D, Baunack S and Schmidt O G 2015 High-performance magnetic sensorics for printable and flexible electronics *Adv. Mater.* **27** 880–5
[71] Krishna V D, Wu K, Perez A M and Wang J-P 2016 Giant magnetoresistance-based biosensor for detection of influenza a virus *Frontiers in Microbiology.* **7** 400
[72] Kokkinis G, Jamalieh M, Cardoso F, Cardoso S, Keplinger F and Giouroudi I 2015 Magnetic-based biomolecule detection using giant magnetoresistance sensors *J. Appl. Phys.* **117** 17B731
[73] Gooneratne C P, Giouroudi I, Liang C and Kosel J 2011 A giant magnetoresistance ring-sensor based microsystem for magnetic bead manipulation and detection *J. Appl. Phys.* **109** :07E517
[74] Lee C-P, Lai M-F, Huang H-T, Lin C-W and Wei Z-H 2014 Wheatstone bridge giant-magnetoresistance based cell counter *Biosens. Bioelectron.* **57** 48–53
[75] Nesvet J, Rizzi G and Wang S X 2019 Highly sensitive detection of DNA hypermethylation in melanoma cancer cells *Biosens. Bioelectron.* **124** 136–42
[76] Gao Y *et al* 2019 Multiplex measurement of twelve tumor markers using a GMR multi-biomarker immunoassay biosensor *Biosens. Bioelectron.* **123** 204–10
[77] Wang W *et al* 2014 Magnetic detection of mercuric ion using giant magnetoresistance-based biosensing system *Anal. Chem.* **86** 3712–6
[78] Julliere M 1975 Tunneling between ferromagnetic films *Phys. Lett. A* **54** 225–6
[79] Miyazaki T and Tezuka N 1995 Giant magnetic tunneling effect in Fe/Al_2O_3/Fe junction *J. Magn. Magn. Mater.* **139** L231–4
[80] Butler W, Zhang X-G, Schulthess T and MacLaren J 2001 Spin-dependent tunneling conductance of Fe| MgO| Fe sandwiches *Physical Review B.* **63** 054416
[81] Mathon J and Umerski A 2001 Theory of tunneling magnetoresistance of an epitaxial Fe/MgO/Fe (001) junction *Physical Review B.* **63** 220403
[82] Sugihara A, Yakushiji K and Yuasa S 2019 Surface smoothing process for high-performance MgO-based magnetic tunnel junctions *Appl. Phys. Express* **12** 023002
[83] Ikeda S *et al* 2008 Tunnel magnetoresistance of 604% at 300 K by suppression of Ta diffusion in Co Fe B／Mg O／Co Fe B pseudo-spin-valves annealed at high temperature *Appl. Phys. Lett.* **93** 082508
[84] Mazumdar D, Liu X, Schrag B, Shen W, Carter M and Xiao G 2007 Thermal stability, sensitivity, and noise characteristics of MgO-based magnetic tunnel junctions *J. Appl. Phys.* **101** 09B502

[85] Ouyang Y, He J, Hu J, Zhao G, Wang Z and Wang S X 2015 Contactless current sensors based on magnetic tunnel junction for smart grid applications *IEEE Trans. Magn.* **51** 1–4
[86] Cubells M *et al* (ed) 2013 *Magnetic Tunnel Junction (MTJ) SENSORS FOR INTEGRATED CIRCUits (IC) Electric Current Measurement. SENSORS* (Piscataway, NJ: IEEE) 2013: IEEE
[87] Jiang Y, Zhang Y, Klemm A and Wang J-P (ed) Fast spintronic thermal sensor for IC power driver cooling down *Electron Devices Meeting (IEDM), 2016 IEEE Int.*2016 (IEEE)
[88] Sengupta A, Liyanagedera C M, Jung B and Roy K 2017 Magnetic tunnel junction as an on-chip temperature sensor *Sci. Rep.* **7** 11764
[89] Cardoso F *et al* 2014 Magnetic tunnel junction based eddy current testing probe for detection of surface defects *J. Appl. Phys.* **115** 17E516
[90] Jin Z, Oogane M, Fujiwara K and Ando Y 2017 Magnetic sensor based on serial magnetic tunnel junctions for highly sensitive detection of surface cracks *J. Appl. Phys.* **122** 174502
[91] Tavassolizadeh A *et al* 2016 Tunnel magnetoresistance sensors with magnetostrictive electrodes: strain sensors *Sensors* **16** 1902
[92] Fuji Y *et al* (ed) 2017 An ultra-sensitive spintronic strain-gauge sensor with gauge factor of 5000 and demonstration of a Spin-MEMS Microphone. Solid-State Sensors, Actuators and Microsystems (TRANSDUCERS) *2017 19th Int. Conf. on*
[93] Fan X *et al* (ed) 2014 Magnetic tunnel junction-based on-chip microwave phase and spectrum analyzer *2014 IEEE MTT-S Int. Microwave Symp. (IMS2014)*
[94] Fu L, Cao Z *et al* 2012 Microwave reflection imaging using a magnetic tunnel junction based spintronic microwave sensor *Appl. Phys. Lett.* **101** 232406
[95] Merazzo K *et al* 2018 Reading magnetic ink patterns with magnetoresistive sensors *AIP Adv.* **8** 056633
[96] Lima E A, Bruno A C, Carvalho H R and Weiss B P 2014 Scanning magnetic tunnel junction microscope for high-resolution imaging of remanent magnetization fields *Meas. Sci. Technol.* **25** 105401
[97] Chen J-Y, Lau Y-C, Coey J, Li M and Wang J-P 2017 High performance MgO-barrier magnetic tunnel junctions for flexible and wearable spintronic applications *Sci. Rep.* **7** 42001
[98] Amara S *et al* 2018 High-performance flexible magnetic tunnel junctions for smart miniaturized instruments *Adv. Eng. Mat.* **20** 1800471
[99] Barraud C *et al* 2010 Magnetoresistance in magnetic tunnel junctions grown on flexible organic substrates *Appl. Phys. Lett.* **96** 072502
[100] Lei Z *et al* 2012 Liver cancer immunoassay with magnetic nanoparticles and MgO-based magnetic tunnel junction sensors *J. Appl. Phys.* **111** 07E505
[101] Sharma P P *et al* 2017 Integrated platform for detecting pathogenic DNA via magnetic tunneling junction-based biosensors *Sensors Actuators B* **242** 280–7
[102] Li F, Kodzius R, Gooneratne C P, Foulds I G and Kosel J 2014 Magneto-mechanical trapping systems for biological target detection *Microchim. Acta* **181** 1743–8
[103] Li F and Kosel J 2014 An efficient biosensor made of an electromagnetic trap and a magneto-resistive sensor *Biosens. Bioelectron.* **59** 145–50
[104] Moretti D *et al* 2018 Biocompatibility of a Magnetic Tunnel Junction sensor array for the detection of neuronal signals in culture *Frontiers in Neuroscience.* **12**
[105] Mohri L V P and High-frequency K 1995 giant magneto-impedance in Co-rich amorphous wires and films *Journal of the Magnetics Society of Japan.* **19** 265–8
[106] Li X *et al* 2018 Magnetoimpedance effect in FINEMET/Ni80Fe20 composite ribbons *J. Alloys Compd.* **730** 17–22
[107] Buznikov N A and Kurlyandskaya G V 2019 Magnetoimpedance in symmetric and non-symmetric nanostructured multilayers: A theoretical study *Sensors* **19** 1761
[108] Vilela G, Monsalve J, Rodrigues A, Azevedo A and Machado F 2017 Giant magnetoimpedance effect in a thin-film multilayer meander-like sensor *J. Appl. Phys.* **121** 124501
[109] Kurlyandskaya G *et al* 2001 Very large magnetoimpedance effect in FeCoNi ferromagnetic tubes with high order magnetic anisotropy *J. Appl. Phys.* **90** 6280–6
[110] Peng H-X, Qin F and Phan M-H 2016 *Ferromagnetic microwire composites: from sensors to microwave applications* (Berlin: Springer)
[111] Panina L and Mohri K 1994 Magneto-impedance effect in amorphous wires *Appl. Phys. Lett.* **65** 1189–91
[112] García-Arribas A *et al* 2013 Tailoring the magnetic anisotropy of thin film permalloy microstrips by combined shape and induced anisotropies *The European Physical Journal B.* **86** 136
[113] Usov N, Antonov A and Lagar'kov A 1998 Theory of giant magneto-impedance effect in amorphous wires with different types of magnetic anisotropy *J. Magn. Magn. Mater.* **185** 159–73
[114] Li B and Kosel J (ed) A thin film passive magnetic field sensor operated at 425 MHz. 2013 Transducers & Eurosensors XXVII *The 17th Int. Conf. on Solid-State Sensors, Actuators and Microsystems (TRANSDUCERS & EUROSENSORS XXVII)*2013 (IEEE)
[115] Uchiyama T, Mohri K and Nakayama S 2011 Measurement of spontaneous oscillatory magnetic field of guinea-pig smooth muscle preparation using pico-tesla resolution amorphous wire magneto-impedance sensor *IEEE Trans. Magn.* **47** 3070–3
[116] Mohri K, Honkura Y, Panina L, Uchiyama T and Super M I 2012 sensor: recent advances of amorphous wire and CMOS-IC magneto-impedance sensor *J. Nanosci. Nanotechnol.* **12** 7491–5
[117] Uchiyama T, Mohri K, Honkura Y and Panina L 2012 Recent advances of pico-Tesla resolution magneto-impedance sensor based on amorphous wire CMOS IC MI sensor *IEEE Trans. Magn.* **48** 3833–9
[118] Mohri K, Uchiyama T, Panina L V, Yamamoto M and Bushida K 2015 Recent advances of amorphous wire CMOS IC magneto-impedance sensors: innovative high-performance micromagnetic sensor chip *Journal of Sensors* **2015** 718069
[119] García-Arribas A, Fernández E and Cos D 2017 Thin-film magneto-impedance sensors *Magnetic Sensors-Development Trends and Applications* (Rijeka: InTech)
[120] García-Arribas A, Fernández E, Svalov A, Kurlyandskaya G and Barandiaran J 2016 Thin-film magneto-impedance structures with very large sensitivity *J. Magn. Magn. Mater.* **400** 321–6
[121] Li B, Kavaldzhiev M N and Kosel J 2015 Flexible magnetoimpedance sensor *J. Magn. Magn. Mater.* **378** 499–505
[122] Karnaushenko D, Karnaushenko D D, Makarov D, Baunack S, Schäfer R and Schmidt O G 2015 Self-assembled on-chip-integrated giant magneto-impedance sensorics *Adv. Mater.* **27** 6582–9
[123] Alfadhel A, Li B, Zaher A, Yassine O and Kosel J 2014 A magnetic nanocomposite for biomimetic flow sensing *Lab Chip* **14** 4362–9
[124] Zhang Y, Mu C, Luo C, Dong J, Liu Q and Wang J 2012 Enhanced giant magnetoimpedance in heterogeneous nanobrush *Nanoscale Res. Lett.* **7** 506
[125] NVE Corporation Corporation N. AA/AB-Series Analog Magnetic Sensors 2019 [Available from (https://nve.com/Downloads/analog_catalog.pdf)

[126] Allegro Microsystems Inc. AAllegro A1324, A1325, and A1326 Low Noise, Linear Hall Effect Sensor ICs with Analog Output 2010-2011 [Available from: (https://alldatasheet.com/datasheet-pdf/pdf/446684/ALLEGRO/A1324.html)
[127] Honeywell International Inc. Honeywell 1-and 2-Axis Magnetic Sensors HMC1001/1002/1021/1022 2008 [Available from: (https://pdf1.alldatasheet.com/datasheet-pdf/view/600478/HONEYWELL-ACC/HMC1002.html)
[128] TE Connectivity Ltd. KMY_KMZ Linear Magnetic Field Sensors 2017 [Available from: (https://eu.mouser.com/datasheet/2/418/NG_DS_KMY_KMZ_A1-1130282.pdf)
[129] Honeywell International Inc. Three-axis Magnetic Sensor HMC1043L 2013 [Available from: (https://media.digikey.com/pdf/Data%20Sheets/Honeywell%20PDFs/HMC1043L.pdf)
[130] Micro Magnetics Inc. Micro Magnetics I. STJ-240 Single-axis Magnetic Sensor 2002-2017 [Available from: (https://micromagnetics.com/docs/STJ-240_datasheet.pdf)
[131] Aichi Steel Corporation Leaflet uT Sensor MI-CB-1DM [Available from: (https://aichi-mi.com/app/download/10314751492/140325_Leaflet_uT+sensor+JPN.pdf?t=1475134861)
[132] Aichi Steel Corporation Nano Tesla Sensor MI-CB-1DH [Available from: (https://aichi-mi.com/app/download/10290224492/Leaflet+MI-CB-1DH.pdf?t=1420787919)